

# Heterodyne swept-source optical coherence tomography for complete complex conjugate ambiguity removal

Anjul M. Davis

Michael A. Choma

Joseph A. Izatt

Duke University

Department of Biomedical Engineering

Durham, North Carolina 27708

E-mail: anjul.m@duke.edu

**Abstract.** Fourier domain (FD) techniques have increasingly gained attention in optical coherence tomography (OCT). This is primarily due to their demonstrated sensitivity of two to three orders of magnitude over conventional time-domain techniques. FDOCT images are subject to two primary sources of artifacts. First, a complex conjugate ambiguity arises because the Fourier transform of the real-valued spectral interferometric signal is Hermitian symmetric. This ambiguity leads to artifactual superposition of reflectors at positive and negative pathlength differences between the sample and reference reflectors. Second, noninterferometric and sample autocorrelation terms appear at dc, obscuring reflectors at zero pathlength difference. We show that heterodyne detection in swept-source OCT (SSOCT) enables the resolution of complex conjugate ambiguity and the removal of noninterferometric and autocorrelation artifacts. We also show that complex conjugate ambiguity resolution via frequency shifting circumvents falloff induced by finite source linewidth in SSOCT when samples are shifted to large pathlength differences. We describe an efficient heterodyne SSOCT design that enables compensation of power losses from frequency-shifting elements. Last, we demonstrate this technique, coupled with wavenumber triggering and electronic demodulation, for *in vivo* imaging of the human anterior eye segment. © 2005 Society of Photo-Optical Instrumentation Engineers. [DOI: 10.1117/1.2136147]

Keywords: optical coherence tomography; medical imaging; ophthalmic imaging.

Paper 05072R received Mar. 18, 2005; revised manuscript received Aug. 12, 2005; accepted for publication Aug. 15, 2005; published online Nov. 18, 2005. This paper is a revision of a paper presented at the SPIE conference on Coherence Domain Optical Methods and Optical Coherence Tomography in Biomedicine IX, Apr. 2005, San Jose, CA. The paper presented there appears (unrefereed) in SPIE Proceedings Vol. 5690.

## 1 Introduction

Fourier domain optical coherence tomography (FDOCT) techniques have reshaped the OCT landscape due to demonstrated sensitivities that are two to three orders of magnitude greater than their time domain counterparts.<sup>1-3</sup> The shift to FDOCT, however, is not without costs. FDOCT techniques are limited in imaging depth and suffer from two important sources of artifacts. The first, called “complex conjugate ambiguity,” arises because the Fourier transform of the real-valued spectral interferometric signal is Hermitian symmetric. This results in sample reflectors at a positive displacement,  $+\Delta x$ , with respect to the reference reflector, being superimposed on those at a negative displacement,  $-\Delta x$ . The second source of artifact, termed “dc artifact,” originates from the noninterferometric light and autocorrelation from sample reflectors, which transform to  $\Delta x=0$ , and thereby obscure reflectors positioned at zero pathlength difference. These artifacts can be removed by retrieval of the complex interferometric signal. Additionally, retrieval of the complex interferometric signal effectively

doubles the imaging depth by removal of the complex conjugate ambiguity.

Previous techniques for acquiring the complex FD interferometric signal have relied on collecting the in-phase and quadrature ( $\pi/2$ -shifted) components generated by phase shifting interferometry<sup>4</sup> or  $3 \times 3$  interferometry.<sup>5,6</sup> These techniques are constrained to homodyne insofar as both the reference and sample arm optical fields have the same phase velocity. Homodyne detection is required for spectral domain OCT (SDOCT) systems that employ spectrometers coupled to charge accumulation detectors such as charge-coupled devices (CCDs) and photodiode arrays. In swept-source OCT (SSOCT), however, a current-generating photodiode is employed, which enables the spectral interferometric signal to be encoded with a characteristic heterodyne beat frequency. Phase-shifting interferometry requires acquisition of multiple images and therefore is not instantaneous.  $3 \times 3$  interferometry is an instantaneous technique for acquisition of the complex interferometric signal. However,  $N \times N$  fiber couplers are wavelength dependent, making it difficult to accurately reconstruct the full complex interferometric signal.

Address all correspondence to Anjul M. Davis, 136 Hudson Hall, Department of Biomedical Engineering, Duke University, Durham, NC 27708. Tel: (919) 660-2475. Fax: (919) 613-9144; E-mail: anjul.m@duke.edu

Two techniques for complex conjugate artifact removal using heterodyne SSOCT have previously been reported. The first described a system utilizing electro-optic phase modulators to introduce a heterodyne beat frequency in the reference arm.<sup>7</sup> A drawback to this technique is that electro-optic modulators are polarization dependent and highly dispersive, thus requiring methods for controlling the polarization and compensation of the group-velocity dispersion. The second technique utilized acousto-optic modulators for heterodyne SSOCT.<sup>8</sup> This system entails an interferometric topology in which the frequency-shifting components are placed between the sample and the receiver. Frequency-shifting elements, such as electro- and acousto-optic modulators, are typically lossy. Placing these elements after the sample prevents the ability to compensate power losses due to light exposure limitations on *in vivo* samples. Additionally, both published techniques required oversampling of the intrinsic signal bandwidth due to the heterodyne modulation, and the latter technique required a computationally intensive algorithm for resampling the acquired data into frequency space.

In this paper, we present a heterodyne SSOCT system that enables efficient detection of the complex interferometric signal, thus having the potential for increased signal-to-noise ratio (SNR). Additionally, we use wavenumber triggering,<sup>9,10</sup> thereby eliminating the necessity to resample the acquired data in software. We show that heterodyne detection in SSOCT enables complete resolution of complex conjugate ambiguity and the removal of noninterferometric signals. We also show that frequency shifting the reference arm optical field upshifts the cross-interferometric signal to a user-tunable frequency that corresponds to an electronic pathlength mismatch between the interferometer arms. This electronic pathlength mismatching recenters the A-scan at an offset that can be far from dc, which effectively resolves the complex conjugate ambiguity problem. While it is also possible, in principle, to upshift the cross-interferometric signal by placing the sample focus at a large pathlength mismatch, this physical pathlength mismatching leads to significant signal attenuation due to amplitude falloff secondary to finite source linewidths.<sup>4,5</sup> We show that frequency shifting provides a method for complex conjugate ambiguity resolution that circumvents signal falloff that occurs by placing samples at a large pathlength mismatch. Through electronic demodulation, we gain access to the in-phase and quadrature components of the interferometric signal and enables wavenumber triggering, which eliminates the necessity for oversampling.

## 2 Theoretical Analysis

### 2.1 Imaging Depth

The imaging depth achieved using FDOCT systems is limited by two mechanisms, the spectral sampling interval (which limits the maximum depth observable) and the system spectral resolution (which leads to a falloff of SNR with depth). The maximum imaging depth in FDOCT systems is described as<sup>2</sup>

$$\Delta z_{\max} = \frac{1}{4\delta_s k}, \quad (1)$$

where  $\delta_s k$  is defined as the spectral sampling interval of the FDOCT system. In SDOCT systems, the spectral sampling

interval is limited by the pixel spacing of the CCD. Reported maximum imaging depths for 1.3  $\mu\text{m}$  SDOCT systems are of the order of 2.0 mm.<sup>11</sup> For SSOCT systems, the spectral sampling interval is limited by the sampling rate of the temporally sweeping source frequency. Over 4.0 mm maximum imaging depths have been achieved for 1.3  $\mu\text{m}$  SSOCT systems.<sup>12</sup>

The second parameter that limits the imaging depth of FDOCT systems is falloff. The sensitivity of FDOCT systems degrades as a function of imaging depth due to fringe wash-out. The  $-3$  dB falloff depth, derived from the analysis reported by Yun et al.<sup>11</sup> is given by

$$\Delta z_{-3\text{dB}} = \frac{2 \ln 2}{\delta_r k}, \quad (2)$$

where  $\Delta z_{-3\text{dB}}$  is the imaging depth at which the SNR is reduced by half, and  $\delta_r k$  is the spectral resolution of the FDOCT system. In SDOCT, the spectral resolution is limited by spectrometer optics and/or the pixel width of the CCD. The preceding expression for the  $-3$  dB falloff point was derived assuming the spectral resolution of SDOCT systems is limited by the Gaussian beam profile in the spectrometer as opposed to the width of the CCD pixel. For SSOCT systems, the spectral resolution is defined by the instantaneous linewidth of the swept laser source. Since spectral sampling and spectral resolution are coupled in spectrometer-based SDOCT systems, they are more limited by falloff compared to SSOCT techniques. The  $-3$  dB imaging depth of a 1.3  $\mu\text{m}$  SDOCT system was reported to be 1.6 mm.<sup>11</sup> In comparison, the  $-3$  dB imaging depth for 1.3  $\mu\text{m}$  SSOCT is 3.7 mm, more than double the distance achieved using SDOCT. Imaging depth capabilities over 4 mm can be valuable for applications such as endoscopy, small animal imaging, and human anterior segment imaging.

### 2.2 Heterodyne SSOCT

In FDOCT, the photocurrent signal generated by  $n$  reflectors is given by

$$i(k) \propto S(k) \left\{ R_R + \sum_n R_n + 2\sqrt{R_R} \sum_n \sqrt{R_n} \cos[2k(z_R - z_n)] + 2 \sum_n \sum_{m \neq n} (R_n R_m)^{1/2} \cos[2k(z_n - z_m)] \right\}. \quad (3)$$

Here,  $i(k)$  is the detector photocurrent as a function of optical wavenumber  $k$ ;  $S(k)$  is the source power spectral density;  $R_R$  and  $R_n$  are the reflectivities of the reference and  $n$ th sample reflector, respectively; and  $z_R$  and  $z_n$  are the positions of the reference and the  $n$ th sample reflector, respectively. The first two terms represent noninterferometric spectral artifacts. The third term represents the cross-interferometric terms, and the fourth term represents the autocorrelation artifact.

In SSOCT systems, the wavenumber is parameterized in time  $t$  by the relationship  $k = k_0 + t(dk/dt)$ , where  $k_0$  is the starting wavenumber, and  $dk/dt$  is the nonlinear sweep velocity. This sweeping leads to the conversion of pathlength differences in the auto- and cross-terms to an electronic frequency in  $i(t)$ , the time-varying photocurrent. The cross-frequencies have instantaneous values of  $\omega_n = (dk/dt)(z_R - z_n)$ , while the autofrequencies have instanta-

neous values of  $\omega_{nm} = (dk/dt)(z_n - z_m)$ . If the reference arm optical field is shifted by some beat frequency  $\omega_D$ , then the time-varying photocurrent becomes

$$i(t) \propto S(t) \left\{ R_R + \sum_n R_n + 2\sqrt{R_R} \sum_n \sqrt{R_n} \cos[(\omega_n + \omega_D)t + \phi_n] + 2 \sum_n \sum_{m \neq n} (R_n R_m)^{1/2} \cos(\omega_{nm} t + \phi_{nm}) \right\}, \quad (4)$$

where  $\phi_n = k_0(z_n - z_m)$  and  $\phi_{nm} = k_0(z_n - z_m)$ . After frequency shifting, the autocorrelation and source spectral terms remain centered at baseband, while the cross-interference terms are recentered around  $\omega_D$ . While the Fourier transform of  $i(t)$  remains Hermitian symmetric, the transform of fringes generated by pathlength differences of equal magnitude but opposite sign no longer overlap. This resolves complex conjugate ambiguity because positive displacements are above  $\omega_D$ , while negative displacements are below  $\omega_D$  as long as  $\omega_D$  is larger than the maximum  $\omega_n$ . If the wavenumber sweep is linear over a bandwidth sweep  $\Delta k$  that takes  $\Delta t$  seconds to complete, then  $\omega_D$  corresponds to a pathlength shift of  $z_D = \omega_D \Delta t / (2\Delta k)$ . This shift does not lead to signal falloff as falloff in SSOCT occurs because the interferometric signal is integrated over the source linewidth at the photodiode. If the source linewidth is of the order of  $2\pi / (z_R - z_n)$ , then the linewidth spans an appreciable portion of the interferometric fringe. This decreases the fringe visibility, which decreases the peak height in the Fourier transform of  $i(t)$ . Frequency shifting creates a time-varying beat frequency that is independent of sweep speed or source linewidth and, as such, it is not susceptible to falloff.

The cross-interferometric signal can be recovered by band-pass filtering around  $\omega_D$  with a noise equivalent bandwidth of  $NEB = 2z_{\max} \Delta k / \Delta t$ . If demodulation is performed the band-passed signal is electronically mixed with orthogonal local oscillators with frequency  $\omega_D$ . In this case, the in-phase (real) and quadrature (imaginary) parts of the complex interferometric signal can be recovered:

$$i_{\text{re}}(t) = 2S(t) \sqrt{R_R} \sum \sqrt{R_n} \cos(\omega_n t + \phi_n),$$

$$i_{\text{im}}(t) = 2S(t) \sqrt{R_R} \sum \sqrt{R_n} \sin(\omega_n t + \phi_n). \quad (5)$$

Additionally, after demodulation, the interferometric signals are dependent only on the time-varying frequency  $\omega_n$ , thereby enabling wavenumber triggering.

### 3 Experimental Setup

We constructed the heterodyne SSOCT setup shown in Fig. 1 using a fiber-based swept laser source (Micron Optics, Inc.,  $\lambda_0 = 1310$  nm,  $\Delta\lambda = 100$  nm, 250 Hz sweep rate), acousto-optic modulators (ACM-1002AA6 IntraAction, Corp.), and a New Focus balanced photoreceiver. The acousto-optic modulators (AOs) had a common center frequency of 100 MHz, one having a user-adjustable offset ( $\omega_D$ ) from that frequency. The diffraction efficiency of the AOs was measured to be 60%, and using the optical setup depicted in the figure, the maximum diffracted optical bandwidth recoupled into the circulator was 64 nm. To trigger each line acquisition, a 250 Hz

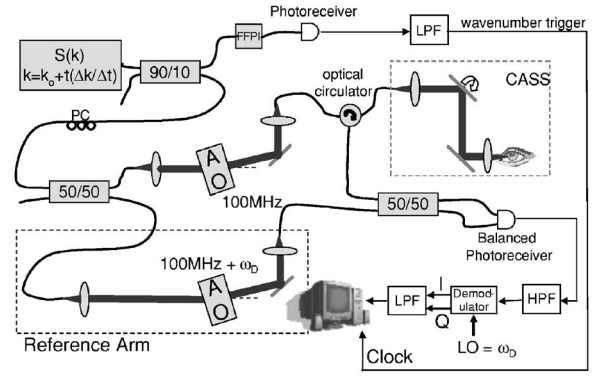


**Fig. 1** Heterodyne SSOCT system utilizing acousto-optic modulators. The swept-laser source has a center wavelength  $\lambda_0 = 1310$  nm and bandwidth  $\Delta\lambda = 100$  nm. A balanced photoreceiver is used for dc artifact suppression. FFPI, fiber Fabry-Pérot interferometer; PC, polarization controllers; AO, acousto-optic modulator; C, circulator; CASS, anterior segment scanner.

clock was provided by the swept-laser source. Spectral interferogram samples evenly spaced in wavenumber were clocked into the data acquisition system by using a fiber Fabry-Perot interferometer (FFPI, Micron Optics, Inc.). Ten percent of the swept-laser source output was delivered to the FFPI and the output was detected using a New Focus 125 MHz photoreceiver. The detected signal was passed through a 2.1 MHz low-pass filter and electronic gain to produce an electronic comb, where each 5 V peak was evenly spaced in wavenumber. The wavenumber spacing was 0.1 nm, given by the free spectral range of the FFPI.

The heterodyne interferometric signal collected using the balanced photoreceiver was high-pass filtered (500 kHz) to remove the spectral and autocorrelation artifacts, then demodulated (RF Micro Devices RF2713) by mixing with a local oscillator (LO) of frequency  $\omega_D$ . The in-phase and quadrature components were low-pass filtered (500 kHz cut-off frequency) and digitized in dual analog-to-digital (A/D) channels (National Instruments PCI 6115) using the clocking signal from the wavenumber trigger. The output power of the swept-laser source was  $500 \mu\text{W}$ . There was approximately  $-6$  dB source power attenuation in the system prior to the sample ( $-3$  dB through the AO and  $-2.9$  dB insertion loss into the fiber of the optical circulator), resulting in  $60 \mu\text{W}$  illumination on the sample (cornea).

The SNR of the system, using a  $-60$  dB calibrated reflector near zero pathlength difference, was measured to be 99 dB. The predicted SNR, assuming same signal power, was 112 dB. The heterodyne SSOCT setup described here, places the AO in front of the sample. This design enables compensation of optical power loss from the AO and, therefore, the SNR of the system could be increased by use of a higher power laser source.

### 4 Results

To illustrate the behavior of the cross-interferometric term in Eq. (3) with the reference arm frequency shifted with respect to the sample arm, we show in Fig. 2 the fringe patterns of typical interferograms at two pathlength differences, centered

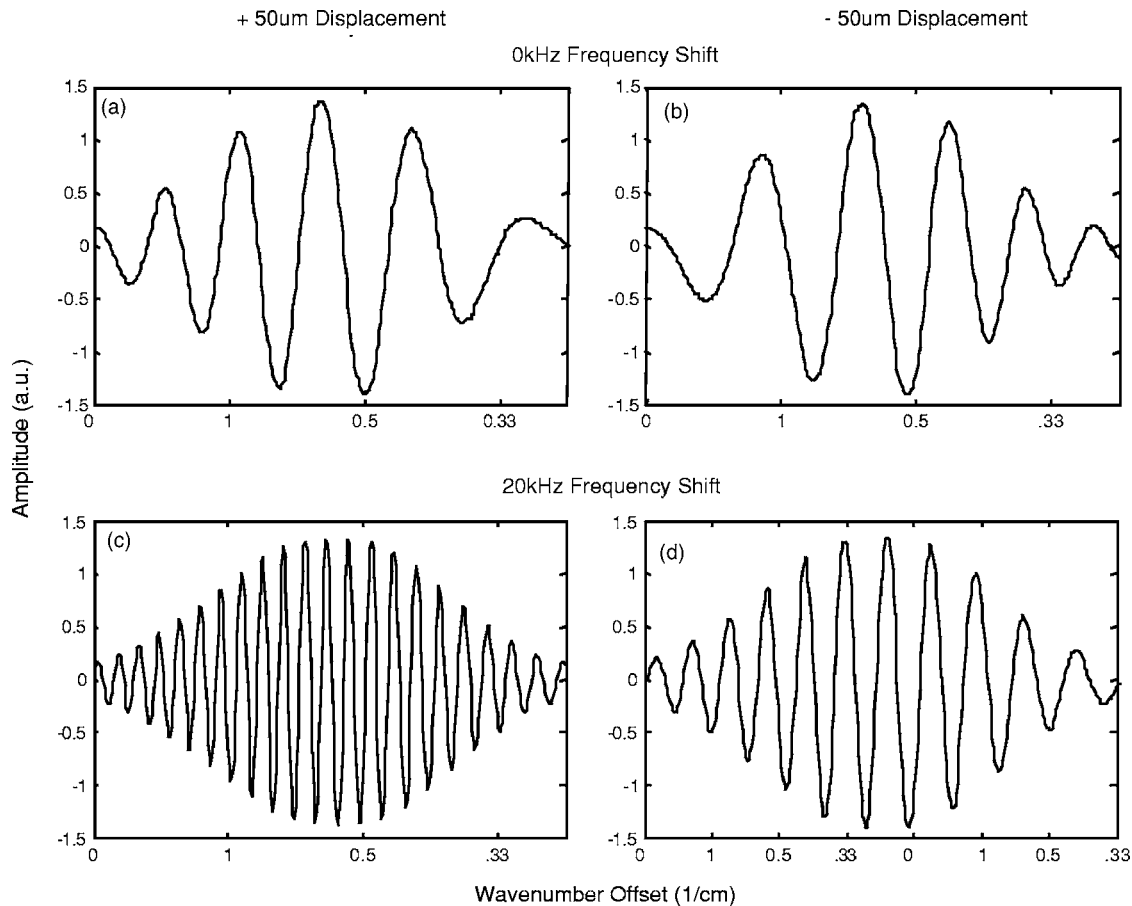


**Fig. 2** Interferograms taken using heterodyne SSOCT: (a) and (b) taken from a reflector at  $+50 \mu\text{m}$  and  $-50 \mu\text{m}$  pathlength difference, respectively, with a 0 kHz frequency shift, and (c) and (d) collected at the same pathlength difference, but with a 20 kHz frequency shift. By using heterodyne detection, reflectors at positive positions produce higher fringe frequencies than those at negative positions and therefore are unambiguously resolved. The chirped signal is a result of wavenumber triggering without demodulation, reinforcing the importance of demodulation when acquiring heterodyne data using a wavenumber trigger.

around zero, for homodyne [Figs. 2(a) and 2(b)] and heterodyne [Figs. 2(c) and 2(d)] SSOCT setups. The homodyne setup was measured by setting  $\omega_D$ , the frequency difference between the two AOs, to zero. The fringe frequency for the cross-correlation term, when  $\omega_D=0$ , was identical for equivalent positive [Fig. 2(a)] and negative [Fig. 2(b)] displacements, and it was thus ambiguous whether the pathlength difference was positive or negative. However, when  $\omega_D=20 \text{ kHz}$ , the fringe frequency for the positive displacement [Fig. 2(c)] was higher than for a negative displacement [Fig. 2(d)], as expected from Eq. (4), and therefore the positive and negative locations were resolved.

Figure 3 demonstrates that the signal falloff remained centered at zero pathlength difference, even as the electronic frequency was shifted. Figure 3(a) shows falloff centered at zero pathlength for homodyne SSOCT. By shifting the zero pathlength difference frequency to  $\omega_D=1 \text{ MHz}$ , the image contents were moved away from dc and bandpass filtered to remove the spectral artifacts. After filtering and demodulation, the falloff was recentered around zero frequency and the  $-3.5 \text{ dB}$  signal attenuation out to a 4.0 mm scan depth was preserved.

In Fig. 4, complete removal of complex conjugate ambiguity and dc artifacts is demonstrated using heterodyne SSOCT. In the A-scan acquired using homodyne SSOCT [Fig. 4(a)], the complex conjugate ambiguity artifact is clearly shown. At zero pathlength difference a strong dc peak from the noninterferometric spectral artifact is also present. By shifting the frequency of the reference arm by  $\omega_D=1 \text{ MHz}$ , the complex conjugate ambiguity was completely resolved [Fig. 4(b)]. Also, the spectral artifact located at dc was removed. There is, however, still present a small dc artifact that originated from the demodulation board. The output signals from the demodulation board contained a small ( $<0.1 \text{ V}$ ) dc offset. As a result, this dc offset appeared as a small peak located at zero pathlength difference in the A-scans. The dynamic range of the system was limited to 25 dB by the input requirements of the demodulation board ( $<80 \text{ mV}$ ). As a result, we were able to demonstrate 25 dB extinction of the complex conjugate ambiguity artifact. In theory, however, the capability of the system to remove this artifact is not limited.

*In vivo* images acquired using homodyne and heterodyne SSOCT techniques are shown in Figs. 5(a) and 5(b), respectively. These images are of the anterior segment of a human

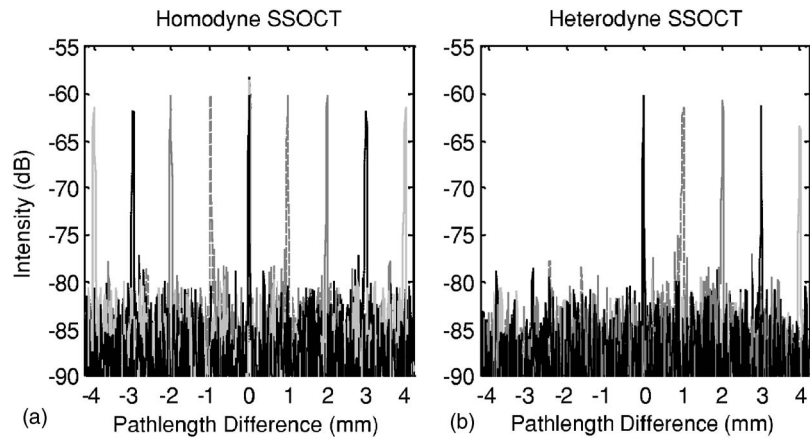


**Fig. 3** Falloff measurements for (a) homodyne and (b) heterodyne SSOCTs acquired using setup in Fig. 1; the  $-3.5$  dB signal falloff was preserved using heterodyne SSOCT;  $-60$  dB calibrated reflector used in sample arm; 1 MHz heterodyne frequency shift.

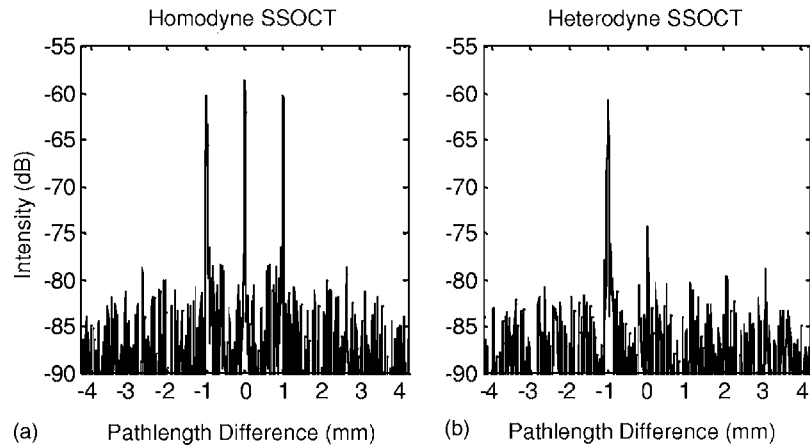


**Fig. 4** A-scans of a  $-60$  dB calibrated reflector at a  $1.0$  mm pathlength difference. (a) A-scan showing unresolved complex conjugate ambiguity acquired using homodyne SSOCT. The complex conjugate ambiguity prevents distinguishing reflectors at a  $+1.0$  mm from those at  $-1.0$  mm pathlength difference. Using heterodyne SSOCT (b), the complex conjugate ambiguity is resolved. The spectral artifact located at dc is also removed, however, a small artifact resulting from a dc offset in the electronic demodulator is present.

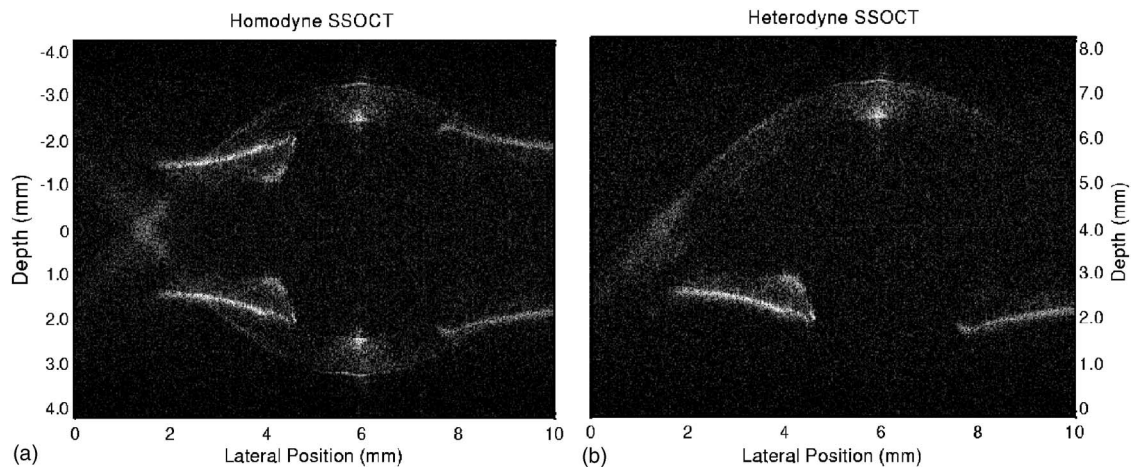


**Fig. 5** *In vivo* images of human anterior segment using (a) homodyne and (b) heterodyne SSOCT techniques. Complete complex conjugate ambiguity removal and doubling of the imaging depth is shown to be necessary in order to visualize the entire anterior segment of the eye. C, cornea; S, sclera; I, iris.

eye and were constructed using 500 lines/image acquired at a rate of 250 Hz. In the homodyne SSOCT image, the iris, cornea, and sclera were obscured by the mirror image arising from the complex conjugate ambiguity artifact. Using heterodyne SSOCT, however, the artifact was completely removed and the cornea, iris, and sclera were no longer obscured. It is evident that at least 6 mm of imaging depth is necessary to visualize the entire anterior segment.

## 5 Conclusions

We demonstrated a heterodyne SSOCT technique using AOs for complex conjugate ambiguity and dc artifact removal. We also presented an efficient heterodyne SSOCT design that minimizes power losses after the sample, enabling an increased SNR. This technique enables the zero pathlength difference to be shifted away from electronic dc with no penalty due to finite laser linewidth falloff. Combined with coherent demodulation, this technique provides access to the entire complex interferometric signal without oversampling, as the method also enables data acquisition using wavenumber triggering, thus eliminating computationally intensive resampling algorithms. Although we had limited available laser source power and dynamic range, we presented a technique for heterodyne SSOCT with wavenumber triggering using electronic demodulation. We also demonstrated *in vivo* human anterior segment images where more than 6 mm imaging depth is required.

## Acknowledgments

This work was supported by National Institute of Health, R21 EB000243. We greatly appreciate the collaboration with K. Hsu at Micron Optics, Inc.

## References

1. R. Leitgeb, C. K. Hitzenberger, and A. F. Fercher, "Performance of Fourier domain vs. time domain optical coherence tomography," *Opt. Express* **11**(8), 889–894 (2003).
2. M. A. Choma, M. V. Sarunic, C. Yang, and J. A. Izatt, "Sensitivity advantage of swept source and Fourier domain optical coherence tomography," *Opt. Express* **11**(18), 2183–2189 (2003).
3. B. R. White, M. C. Pierce, N. Nassif, B. Cense, B. H. Park, G. J. Tearney, B. E. Bouma, T. C. Chen, and J. F. de Boer, "*In vivo* dynamic human retinal blood flow imaging using ultra-high-speed spectral domain optical Doppler tomography," *Opt. Express* **11**(25), 3490–3497 (2003).
4. M. Wojtkowski, A. Kowalczyk, R. Leitgeb, and A. F. Fercher, "Full range complex spectral optical coherence tomography technique in eye imaging," *Opt. Express* **27**(16), 1415–1417 (2002).
5. M. A. Choma, C. Yang, and J. A. Izatt, "Instantaneous quadrature low-coherence interferometry with  $3 \times 3$  fiber-optic couplers," *Opt. Lett.* **28**(22), 2162–2164 (2003).
6. M. V. Sarunic, M. A. Choma, C. Yang, and J. A. Izatt, "Instantaneous complex conjugate resolved spectral domain and swept-source OCT using  $3 \times 3$  fiber couplers," *Opt. Express* **13**(3), 957–967 (2005).
7. J. Zhang, J. S. Nelson, and Z. Chen, "Removal of a mirror image and enhancement of the signal-to-noise ratio in Fourier-domain optical coherence tomography using electro-optic phase modulator," *Opt. Lett.* **30**(2), 147–149 (2005).
8. S. H. Yun, G. J. Tearney, J. F. de Boer, and B. E. Bouma, "Removing the depth-degeneracy in optical frequency domain imaging with frequency shifting," *Opt. Express* **12**(20), 4822–4828 (2004).
9. M. A. Choma, M. V. Sarunic, C. Yang, K. Hsu, and J. A. Izatt, "Sensitivity advantage of swept source and Fourier-domain optical coherence tomography," presented at Coherence Domain Optical Methods and Optical Coherence Tomography in Biomedicine VIII, Jan. 24–29, 2004, San Jose, California, SPIE.
10. M. A. Choma, K. Hsu, and J. A. Izatt, "Swept source optical coherence tomography using an all-fiber 1300-nm ring laser source," *J. Biomed. Opt.* **10**, 044–009 (2005).
11. S. H. Yun, G. J. Tearney, B. E. Bouma, B. H. Park, and J. F. de Boer, "High-speed spectral domain optical coherence tomography at 1.3  $\mu\text{m}$  wavelength," *Opt. Express* **11**(26), 3598–3604 (2003).
12. A. Maheshwari, M. A. Choma, and J. A. Izatt, "Heterodyne swept-source optical coherence tomography for complete complex conjugate ambiguity removal," in *Coherence Domain Optical Methods and Optical Coherence Tomography in Biomedicine IX, Proc. SPIE* **5690**, 91–95 (2005).